THE JOURNAL OF PHYSICAL CHEMISTRY C

Article

pubs.acs.org/JPCC

Effect of Roughness on the Microscale Friction of Hydrocarbon Films

Steven G. Vilt,[†] Christopher J. Caswell,[†] Juan C. Tuberquia,[†] Clare McCabe,[†,‡] and G. Kane Jennings*[,†]

[†]Department of Chemical and Biomolecular Engineering and [‡]Department of Chemistry, Vanderbilt University, Nashville, Tennessee 37235, United States

ABSTRACT: To investigate polymer friction and the role of surface roughness on polymer tribology, microtribometry testing was performed using hydrocarbon films ranging in roughness from a molecularly smooth monolayer to extremely rough polymethylene coatings that were prepared on both the substrate (a flat silicon wafer) and the probe (a 6 mm borosilicate lens). The results show that the rough topography of the polymer films dramatically increases frictional forces when both the probe and substrate contain rough films, but if one surface contains a hydrophobic, smooth monolayer, friction values are greatly reduced. In addition, tribometry tests were performed with the substrates submerged under water to examine the tribometric influence of the testing medium and to determine whether hydrophobic interactions are relevant on the microscale. At the loads and speeds tested, hydrophobic interactions did not significantly affect the frictional properties between the coated probe and substrate in water. The hydrophilic control probe, in contrast, showed decreased frictional forces for the polymer substrates in the water environment, consistent with an adsorbed, lubricating water layer.

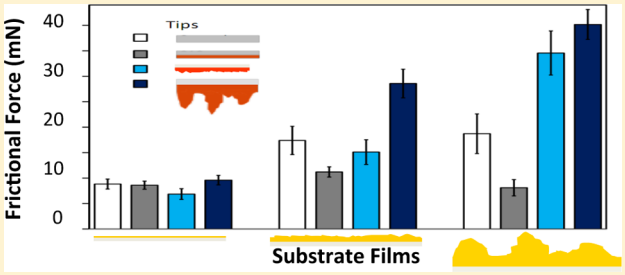

INTRODUCTION

Polymer coatings have generally shown poor lubricating performance[1] due to their inherent roughness, which results in deformation of surface asperities, commonly referred to as plowing.[2,3] The majority of microscale frictional investigations involving polymers has been conducted with smooth probe surfaces, usually a metal ball or polymer pin, such that little is known regarding how surface morphology influences the tribological properties of two polymer coatings sliding across each other. Compared to a smooth probe, a rough polymer probe contacting a polymer surface presents different frictional mechanisms as contacting asperities can penetrate into each other and ratchet over each other.[4] An improved understanding of how coating and probe roughness—from molecularly smooth surfaces to those with varied levels of surface roughness—affect frictional performance is needed.

To investigate the effects of surface energy and topography on polymer/polymer friction, we have conducted tribometry experiments utilizing a variety of probe and substrate films. In addition to the unmodified probe, which is an unmodified silica lens, three hydrocarbon films that vary in their roughness were deposited on the probe and substrates: a solidlike monolayer prepared from octadecyltrichlorosilane (C18) that is molecularly smooth,[5] a polymethylene (PM) film prepared by surface-catalyzed polymerization from gold[6,7] that has nanoscale roughness, and a superhydrophobic polymethylene (SH) film prepared by surface-initiated polymethylenation[7,8] on gold that has microscale roughness. Thus, the C18, PM, and SH films all expose low-energy hydrocarbon surfaces but vary immensely in their surface topographies. In addition, the polymers are semicrystalline films that contain 70% orthorhombic crystalline content[8] as well as amphorous domains, in contrast to the oriented, crystalline C18 monolayer. All testing was completed at room temperature (22 °C), which is much greater than the glass transition temperature for polymethylene (−120 °C),[9] and therefore, the polymer film will contain chains that have liquidlike movement under shear.[10,11]

Frictional testing was also performed while the substrates were submerged in water. Underwater testing allows the investigation of the influence of hydrophobic interactions on microscale friction, the effectiveness of an entrapped air lubrication layer at the SH interface, and the frictional benefit of an adsorbed water layer. Chemical force microscopy studies have shown that hydrophobic interactions play an important role in nanoscale frictional measurements;[12,13] however, their importance has not been assessed in microtribometry. The SH films studied, while composed of hydrophobic PM, provide an interface vastly different from those of the C18 and PM films. When submerged in water, the SH films will harbor a micrometer-thick film of air, creating a polymer/water interface that consists mainly of entrapped air.[7] As two superhydrophobic surfaces come into contact under water, pockets of air form between the two surfaces[14] and are known to enhance interfacial slip lengths for water[15] and dramatically increase attractive forces between approaching superhydrophobic substrates in water;[16,14] however, their effect on solid/solid friction in a water phase has not been established. Our investigation will determine if the entrapped air can alter friction between sliding surfaces at the microscale. Lastly, the hydrophilic control probe provides an opportunity to

Received: June 5, 2012
Revised: September 10, 2012
Published: September 18, 2012

investigate the influence of an adsorbed water layer on microtribometry. Thin films of water are known to be effective lubricating layers,[17] and introducing water into the lubrication systems could reduce frictional forces and provide additional insight into polymer friction.

EXPERIMENTAL METHODS

Materials. *n*-Octadecyltrichlorosilane was purchased from United Chemical Technologies. Hydrogen peroxide (H_2O_2; 30%) and toluene were purchased from Fisher Scientific. Sulfuric acid (H_2SO_4) was purchased from EMD Chemicals, Inc. Ethanol (ACS/USP grade) was purchased from AAPER. All reagents and chemicals were used as received. Undec-10-ene-1-thiol was synthesized with detailed protocols outlined in previous works.[7,18] Diazomethane (DM) was carefully synthesized according to the literature to produce a ca. 16 mM solution in diethyl ether[19] and stored at −17 °C. Borane−tetrahydrofuran (THF) complex solution (1.0 M) was acquired from Sigma-Aldrich. N-BK7 plano-convex lenses with a diameter of 6 mm and a radius of curvature of 15.5 mm were obtained from Thorlabs. Gold shot (99.99%) and chromium-coated tungsten filaments were purchased from J&J Materials and R. D. Mathis, respectively. Silicon (100) wafers were obtained from Wafer Reclaim Services, LLC.

Preparation of Silicon Substrates. Silicon wafers were first cut into 4 cm × 1.3 cm pieces using a diamond-tip stylus. The silicon samples were sequentially rinsed with ethanol and water and again with ethanol, dried in a stream of N_2, and then sonicated in ethanol for 30 min to displace any remaining contaminants. After sonication, the samples were rinsed sequentially with water and ethanol, dried in a stream of N_2, and placed in piranha solution (14 mL of concentrated H_2SO_4/ 6 mL of 30% H_2O_2(aq)) for 30 min to hydroxylate the silicon oxide surface. The piranha-treated substrates were rinsed three times by submersion in water. All samples were rinsed once more in a stream of deionized (DI) water, briefly rinsed with ethanol, and thoroughly dried with N_2 before testing or submersion in the precursor solution. Using an atomic force microscope, the root-mean-square roughness of the silicon substrate was determined to be 1.8 ± 0.3 nm over a 10 μm × 5 μm area.

Preparation of Silica Lenses. The silica lenses were rinsed sequentially with water and ethanol, dried in a stream of N_2, and placed in piranha solution for 30 min to hydroxylate the glass surface. The piranha-treated substrates were rinsed three times by submersion in water. All samples were rinsed once more in a stream of DI water, briefly rinsed with ethanol, and thoroughly dried with N_2 before submersion in the precursor solution.

Preparation of Gold Substrates and Gold-Coated Tips. Silicon (100) wafers and silica lenses were rinsed with water and ethanol and dried in a stream on N_2 prior to being placed in a metal atom evaporator and reducing the pressure to 5 × 10^{-4} Pa with a diffusion pump. Then chromium (100 Å) and gold (1250 Å) were evaporated in sequence onto the wafers and lenses at rates of 1−2 Å s^{-1}. The chamber was then brought to atmospheric pressure, and the gold-coated silicon wafers and silica lenses were removed. The wafers were cut into 1.2 cm × 4 cm samples. The gold-coated substrates and lenses were rinsed with ethanol and dried with N_2 before use.

Formation of C18 Monolayers. The monolayers were formed by immersing the piranha-treated silicon substrates and silica lenses into 1 mM solutions of *n*-octadecyltrichlorosilane in toluene. After 5 h, the samples were removed from the solution, rinsed in ∼20 mL of toluene for 1 min, sequentially rinsed with ethanol and water and again with ethanol, and dried in a stream of N_2. Then they were stored in capped glass vials (substrates) or capsules (probes) until characterization or testing was performed.

Formation of PM Films. PM films were prepared by immersing the gold-coated silicon substrate and gold-coated silica lenses in a 16 mM DM solution in ether for 24 h at −17 °C. Upon removal from the solution the samples were rinsed with ethanol and dried in a stream of nitrogen.

Formation of SH Polymethylene Films. The SH films were prepared by first assembling a vinyl-terminated self-assembled monolayer (SAM). Vinyl-terminated SAMs on the gold-coated substrates and lenses were prepared by immersing the samples for 12 h in a 1 mM undec-10-ene-1-thiol solution in ethanol. After removal from the thiol solution, the samples were rinsed with ethanol and dried with nitrogen. The vinyl monolayer was then placed under nitrogen in a septum-capped vial by three cycles of evacuation followed by nitrogen backfilling. A 0.1 M solution of borane in THF was added to the vial via cannula. After 2 h of reaction, the borane solution was evacuated from the system, and the samples were rinsed three times with anhydrous THF via cannula. Finally, the samples were immersed in a 16 mM DM solution in ether at −17 °C for 3 h, and upon removal from the DM solution, the samples were rinsed in streams of trichlorobenzene and ethanol and dried in a stream of nitrogen.[8]

Profilometry. Profilometry measurements were performed in a Veeco Dektak 150 profiler using 49 μN of force and the hills and valleys detection mode. Thickness was estimated by scratching the surface, scanning 1 mm across the scratch, and plane-fitting the scan results using the instrument software. Reported errors represent the averages and standard deviations of six independently prepared films.

Ellipsometry. Ellipsometric thicknesses were determined from a J. A. Woollam XLS-100 variable-angle spectroscopic ellipsometer. Three separate thickness measurements were taken at different locations across each sample, and the resulting average was reported as the thickness of the monolayer. Thicknesses were fit to data taken at 75° from the surface normal over wavelengths from 200 to 1000 nm. For the monolayers formed on silicon substrates, the sample was modeled as a 0.5 mm Si substrate with an oxide layer and a Cauchy layer.[20] The thickness of the oxide layer was approximated by measuring a piranha-treated silicon sample obtained fresh each time films were measured. The index of refraction was set to 1.46, and the second Cauchy coefficient was set to 0. For the PM films created on the gold-coated substrates, a fresh and uncoated substrate served as a baseline for thickness measurements and was used to determine the optical constants of the substrate. The film thickness was estimated using the Cauchy model with the index of refraction set to 1.52 and the second coefficient set to 0.[21] All films were fit using the software's "normal fit" application. The reported values and errors reflect the average and standard deviation of at least five independently prepared films.

Contact Angles. Advancing and receding contact angles of water and hexadecane were measured with a Rame-Hart manual contact angle goinometer. Contact angles were obtained on both sides of approximately 10 μL drops with the syringe in the probe droplet during measurements. The

Table 1. Thicknesses, Roughnesses, and Water and Hexadecane Contact Angles for the Various Films Deposited on the Substrate and Probe Surfaces

			θ_W (deg)		θ_{HD} (deg)	
	thickness[a] (nm)	roughness (nm)	adv	rec	adv	rec
unmodified tip		1.4 ± 0.5	54 ± 3	31 ± 4	<5	
C18 substrate	2.6 ± 0.2	1.7 ± 0.3	110 ± 1	103 ± 2	44 ± 1	41 ± 1
C18 tip			110 ± 1	102 ± 2	43 ± 2	40 ± 2
PM substrate	76 ± 10	14 ± 3	120 ± 5	61 ± 4	<5	
PM tip			122 ± 3	62 ± 5	<5	
SH substrate	1,721 ± 115	161 ± 87	164 ± 3	160 ± 3	<5	
SH tip			157 ± 2	152 ± 3	<5	

[a]The thicknesses of the C18 and PM films were determined from ellipsometry, while the thickness of the SH film was determined using profilometry.

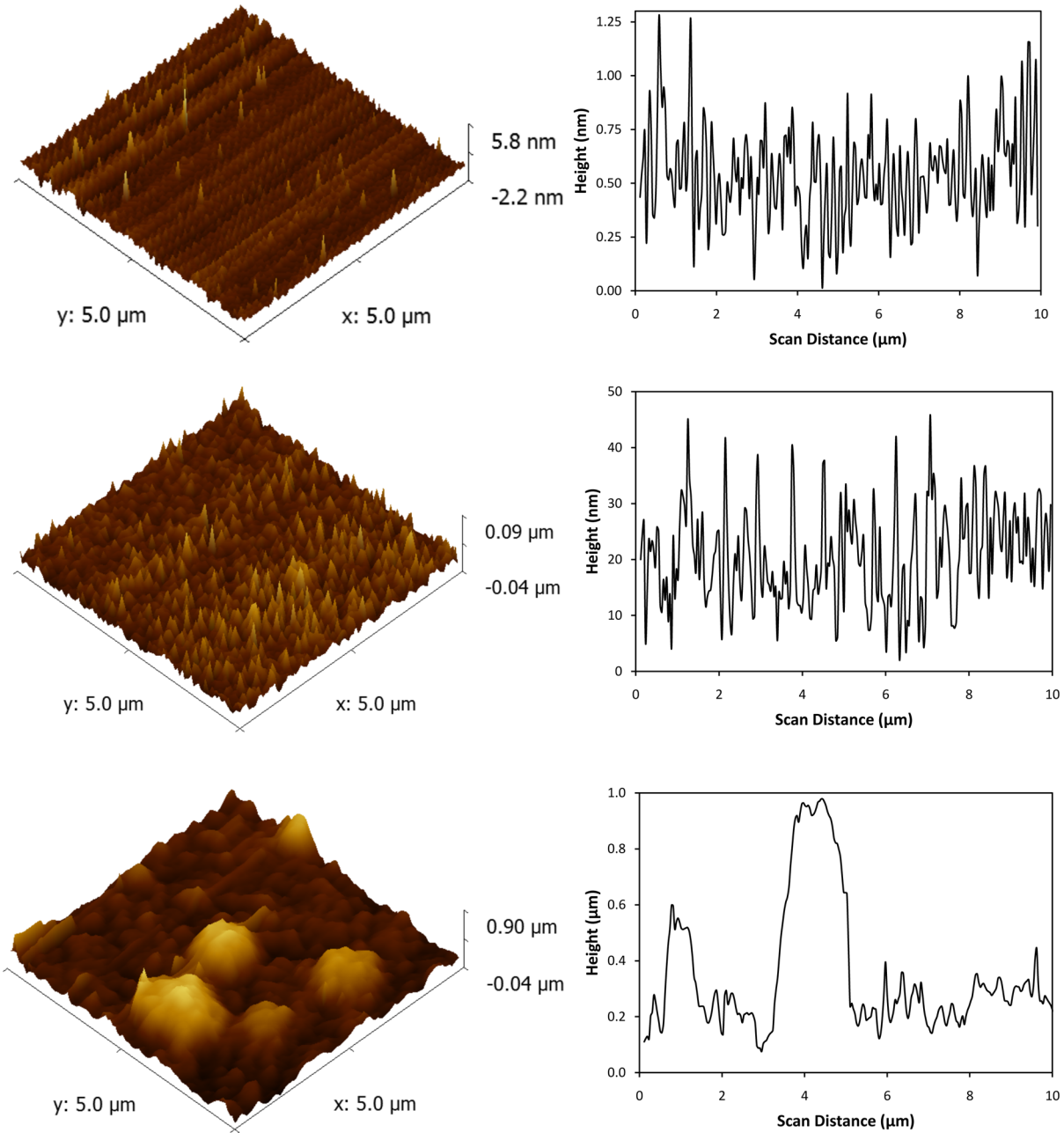

Figure 1. Tapping mode AFM images and line scans of the C18 monolayer (top), polymethylene film (middle), and superhydrophobic film (bottom).

dx.doi.org/10.1021/jp305527h | J. Phys. Chem. C 2012, 116, 21795−21801

reported values and errors reflect the average and standard deviation of at least five independently prepared films.

Microscale Friction Testing. Microscale friction tests were performed either in open air or with the sample immersed in water. Testing in water was accomplished by constructing a custom-made container that allowed the sample to be anchored to the tribometer stage while submerged under a depth of ~5 mm of water. Testing was conducted with a ball-on-flat microtribotester (Center for Tribology, Inc.) using a DFM-0.5 force sensor. The DFM sensor can apply loads from 50 mN to 50 N and was used to perform single-pass friction tests with a constant load of 98 mN. This low load, at which a C18 monolayer can withstand 50 h of sliding,[22] was selected to negate any measurement effects due to different strengths and load-carrying capacities of the films. The probe tip was a borosilicate glass lens that was affixed on a stainless steel rod. All single-pass tests were conducted with a sliding speed of 0.1 mm/s and a scan length of 15 mm. Three tests were performed on each sample, and the reported frictional force (F_f) was determined by averaging the forces measured during the three tests. The reported values and errors reflect the average and standard deviation of at least three different frictional traces at different locations on each of at least three independently prepared films. The measured frictional force (F_f) can be related to the coefficient of friction (μ) by Amonton's law as[18]

$$F_f = \mu F_N + F_0 \quad (1)$$

where F_N is the normal force and F_0 is the residual force typically arising from the adhesion between the probe tip and surface. As the residual force is negligible for low-energy surfaces but not for some high-energy surfaces,[18] we have reported the measured frictional forces rather than the coefficients of friction for this diverse array of probe and substrate surfaces. Nonetheless, for an estimate of the coefficient of friction for low-energy surfaces, assuming F_0 is negligible, one can divide the measured frictional force for each probe/film combination by the normal load of 98 mN.

RESULTS AND DISCUSSION

Characterization of Surfaces. Three different hydrocarbon films were deposited on the probe lenses and substrate surfaces: a monolayer film assembled from C18,[18] a PM film grown from diazomethane precursors on gold via a surface-catalyzed polymerization,[6,7] and a microscopically rough SH film grown by a surface-initiated polymerization.[7,8] The C18 monolayers were formed on the glass probe and silicon substrates by hydroxylating the surfaces and immersing them in a solution containing the trichlorosilane precursor. The two different polymerization processes required a gold surface, and therefore, the glass lenses and silicon substrates were coated with a 125 nm gold layer before the PM and SH films were assembled onto the surfaces. We have previously shown that monolayer films of similar thickness deposited on gold versus silicon exhibit the same coefficients of friction in single pass testing, suggesting no role of the substrate.[23]

The films were characterized by ellipsometry/profilometry and contact angles to assess the thickness and wettability of the films (Table 1), as well as atomic force microscopy (AFM) to investigate the topography of the resulting surfaces (Figure 1). Thicknesses of the probe films could not be determined due to the curvature of the lenses. The ellipsometric thickness of the C18 substrate monolayer was 2.6 ± 0.2 nm, and the advancing (adv) and receding (rec) contact angles for the substrate were statistically the same as those for the probe.The contact angles signal that comparably dense and oriented monolayers were formed on both the substrate and probe surfaces.[18,24,25] An AFM image and line scan of the C18 substrate monolayer (Figure 1 (top)) reveal a molecularly smooth surface with peak heights on the scale of ~1 nm. The roughness of this surface (1.7 ± 0.3 nm) is comparable to that for the uncoated silicon surface (1.8 ± 0.3 nm).

The two polymethylene films (PM and SH) differ considerably in thickness and in topography. The ellipsometric thickness of the PM substrate films was measured as 76 ± 10 nm. The water contact angles for the substrate and probe PM films are in statistical agreement at 120 ± 5° (adv) and 61 ± 4° (rec) and 122 ± 3° (adv) and 62 ± 5° (rec), respectively, while the HD contact angles are <5° for all. The elevated advancing water contact angles and high hysteresis are consistent with a surface that features nanoscale asperities, in agreement with Figure 1 (middle), which shows a surface of nanoscale roughness (rms roughness 14 ± 3 nm) and feature asperities that are 10−50 nm in height. The SH films were too rough for ellipsometric measurements, and therefore, profilometry was used to determine the thickness of these films. The average thickness of the SH films was determined to be 1720 ± 115 nm. The water contact angles for the SH films are considerably higher than those for the PM films, as the SH substrate exhibits values of 164 ± 3° (adv) and 160 ± 3° (rec) while the probe SH surface has values of 157 ± 2° (adv) and 152 ± 3° (rec), both sets justifying the classification as superhydrophobic. The SH films possess a combination of micrometer- and nanoscale features (Figure 1 (bottom)) that give the films their superhydrophobic properties.[8] When a drop of water is placed onto the rough surface, a majority of the polymer interface is occupied by air pockets,[26] resulting in the water drop contacting less than 5% of the polymer interfacial area (~95% air), on the basis of analysis with the Cassie equation.[8]

Polymer Friction. *Effect of the Probe Surface Composition.* To investigate the tribological interactions of two sliding polymer surfaces and the role of surface roughness on polymer friction, microtribometry testing was performed using a variety of probe tips and substrates in ambient air. A common equation to describe polymer friction is the Bowden and Tabor adhesion model:[27]

$$F_f = \tau A_r + F_p \quad (1)$$

where τ is the shear strength of the surface, A_r is the real area of contact, and F_p is the plowing force due to the deformation of asperities.[27] Due to the microscale asperities of the SH film, ratcheting is an additional mechanism of friction that is possible. Ratcheting occurs when one asperity has to climb over the other as the surfaces slide and is prominent when microscale asperities are present.[28] The frictional forces in the polymer systems, therefore, will arise from three main factors: adhesion, which occurs at the real area of contact between the probe and substrate, plowing of asperities, and ratcheting.[4,27,29] These frictional mechanisms are additive[4] and can be related to the friction force (F_f) through the equation

$$F_f = \tau A_r + F_p + F_r \quad (2)$$

where F_r is the ratcheting force.[4] The effects of plowing and ratcheting can qualitatively be observed in Figure 2, which shows the test profiles obtained with an unmodified glass probe on the C18, PM, and SH films, along with a plain silicon substrate for comparison. As can be seen from the figure, rather

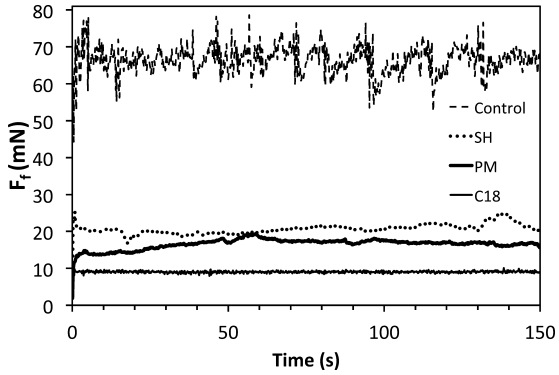

Figure 2. Effect of the substrate film on the frictional forces obtained with an unmodified borosilicate lens of 6 mm diameter at a sliding speed of 0.1 mm/s and a 98 mN load. The tribological test represents a single pass over a distance of 1.5 cm. The control is an unmodified silicon substrate.

than the continuous smooth sliding profile that is achieved with monolayer friction (C18), the polymer data are more erratic.

The tribometry results for all four probe surfaces (unmodified, C18, PM, and SH) on the three substrate films are compared in Figure 3. The frictional data obtained with the

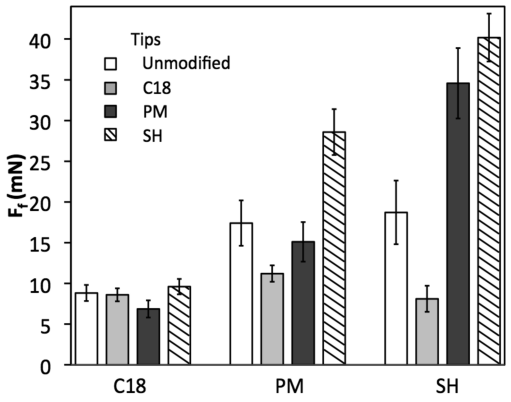

Figure 3. Effect of probe and substrate coatings on the friction force. The single-pass tribology tests were performed in air at 0.1 mm/s with a scan length of 15 mm. Tests on the three hydrocarbon substrate films (C18 monolayer, PM, and SH) were performed with either an unmodified lens or lenses coated with one of the three hydrocarbon films. Reported values and error bars represent averages and standard deviations, respectively, based on at least three different measurements on each of at least three independently prepared films.

unmodified and C18 probes will be discussed first, as these surfaces are both molecularly smooth (with rms values of <2 nm), allowing us to isolate the influence of the surface energy of the probe on polymer friction. First, Figure 3 shows that the smooth C18 monolayer as substrate exhibits the same low frictional forces regardless of whether the probe is a hydrophobic C18 monolayer or an unmodified hydrophilic glass surface. Nonetheless, the surface energy of the probe has a significant influence when the substrate is a polymer film. For the PM films, the friction force is reduced from 17.4 ± 2.7 mN with an unmodified probe to 11.2 ± 1.0 mN with a low-energy C18 probe. The SH films show an even greater decrease, as the friction is reduced from 18.7 ± 3.9 mN (unmodified probe) to 8.1 ± 1.6 mN (C18 probe). Even though the C18 and polymer films are all low-energy hydrocarbon films, the polymer substrates have a greater dependence on the probe surface energy because of the differences in morphology. The smooth and crystalline C18 monolayer[30] does not undergo significant deformation, which creates a low-shear surface that undergoes negligible plowing. In contrast to the well-ordered[5,31] and solidlike C18 monolayer,[30] the polymer films are semicrystalline[8] and contain amphorous domains. Tribometry testing was conducted at room temperature, which is substantially greater than the glass transition temperature for polyethylene (−120 °C),[9,32] and therefore, the chains in the amphorous domain of the polymer material are in a liquidlike state[10,11] and allow greater penetration of the probe into the film,[33] increasing the shear strength.[2] More significantly, the polymer films contain asperities that will deform during sliding and drastically increase the friction force due to plowing.[28] Since the polymer films have higher shear strength and undergo plowing, the probe surface energy has a greater significance. Therefore, when a C18 monolayer is used as the probe, its lubricating properties[18,23,34,35] diminish the plowing force and shear strength for the polymer substrates, resulting in decreased frictional forces compared to those of the unmodified probe.

The SH films are substantially rougher than the PM films and contain microscale asperities (Figure 1), yet the friction force values obtained with the unmodified probe for the SH and PM films are statistically indistinguishable. Furthermore, the SH films actually achieve lower frictional forces than PM films when the C18 probe is used (8.1 ± 1.6 mN vs 11.2 ± 1.0 mN). Here, the microscale asperities of the SH film limit the real contact area between the probe and the SH film since the probe will only contact the summit of the asperities.[28] The decrease in real contact area will decrease adhesion[36,37] and in turn will offset the increase in plowing force brought on by the asperities, resulting in similar friction force values for the PM and SH substrates.[28]

Effect of Polymer Probes. Compared to the smooth unmodified and C18 lenses with roughnesses of 1.4 and 1.7 nm, respectively, testing with probes containing polymer films provides significantly different surface contacts and interfacial interactions. In Figure 3 the effect of the polymer probe on the frictional forces depends on the contacting substrate. The SH substrates exhibit the largest dependence on the probe, as the PM probes produce a friction force of 34.6 ± 4.3 mN and the SH probes result in frictional forces of 40.2 ± 2.9 mN, which are much higher than the friction force measured with the unmodified probe (18.7 ± 2.9 mN) or the C18 probe (8.1 ± 1.6 mN). The PM substrate achieves similar friction forces with the unmodified and PM probe (17.4 ± 2.7 and 15.1 ± 2.4 mN, respectively), but the SH probe produces a significantly higher friction force of 28.6 ± 2.8 mN. Unlike the polymer substrates, the frictional performance of the C18 substrate is relatively insensitive to the probe surface, as the frictional forces are between 6.9 and 9.6 mN for all probes.

The frictional behavior for the polymer-coated probes is driven by the plowing of asperities and the ratcheting mechanism. The plowing force will be increased for polymer/polymer systems since both surfaces contain asperities that can penetrate into the interfacial region.[38] The ratcheting effect will be more prominent when microscale asperities are present;[28] thus, the highest friction forces occur for the SH (probe)/SH (substrate) system, followed by the PM/SH and SH/PM systems. When the ratcheting effect is negligible, as it would be for the PM/PM, SH/C18, and PM/C18 systems, the polymer probes produce much lower frictional forces. For the PM

dx.doi.org/10.1021/jp305527h | J. Phys. Chem. C 2012, 116, 21795−21801

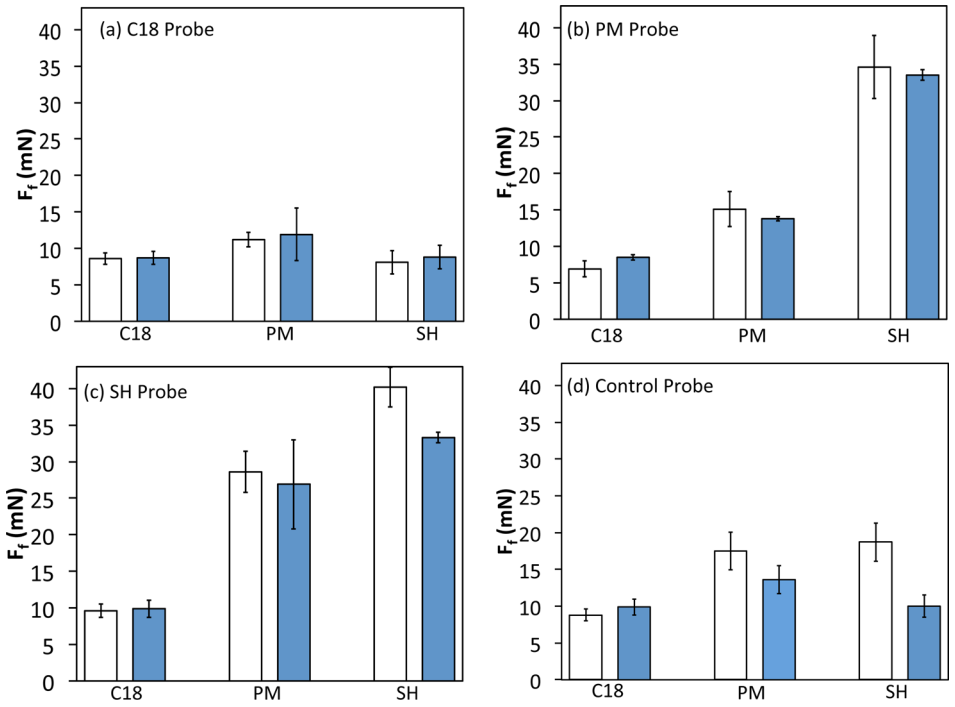

Figure 4. Frictional effect of water submersion for the (a) C18, (b) PM, (c) SH, and (d) control probes on C18, PM, and SH films. The single-pass tribology tests were performed at 0.1 mm/s with a scan length of 15 mm. Testing was done either in ambient air (white) or while the substrate was submerged in water (blue). Reported values and error bars represent averages and standard deviations, respectively, based on at least three different measurements on each of at least three independently prepared films.

substrate, the PM probe produces a slightly lower frictional force than the unmodified probe and provides evidence that the reduction in adhesion between two low-energy PM surfaces is significant and can offset the increase in plowing force due to the addition of another rough polymer surface. Compared to the polymer/polymer systems, tests conducted on the C18 substrate show decreased plowing forces since only one surface would contain asperities. This decrease in plowing and the low-energy surfaces of the polymer probes allows the SH probe to achieve friction forces similar to those of the unmodified probe (9.6 ± 0.9 and 8.8 ± 1.0 mN, respectively) and the PM probe to achieve the lowest friction forces at 6.9 ± 1.1 mN. Considering the combined results of the C18 probe and C18 substrate, the frictional benefit of a solid, smooth, and low-energy monolayer[18,34] when the other contacting surface is a rough polymer or a high-energy surface is clearly shown.

Effect of the Testing Medium. To examine the tribometric influence of the testing medium and to determine whether entrapped air and hydrophobic interactions have a significant influence on microtribometry results, frictional tests were also performed with the substrates submerged under ∼5 mm of water. Figure 4 compares the air and water frictional results for the various systems. For the C18 and PM probes, the testing environment had no influence on the frictional results, as the frictional forces are nearly identical in water and in air for all substrates (Figure 4a,b). These tests involve two hydrophobic surfaces coming into contact under water, and therefore, the hydrophobic effect will cause additional adhesion.[12,14] At the nanoscale, adhesive forces from different testing media can differ by 2 orders of magnitude and can have a considerable influence on AFM frictional measurements.[12] The results shown here signify that hydrophobic interactions are insignificant at the higher loads and larger size scale of microtribometry.

The superhydrophobic properties of the SH probe will create an interface different from that of the C18 or PM probe. The microscale asperities of the SH film create air pockets when the surface is in contact with water, and therefore, air will be entrapped between the water and polymer interface once the superhydrophobic film is submerged under water.[7] At the nanoscale the air pockets have significantly influenced the tribological properties of superhydrophobic substrates,[14,16] and these surfaces have been used to achieve low-friction fluid flow.[39,40] When two superhydrophobic surfaces approach in water, 30-fold greater adhesion forces have been observed, as well as cavitation of the water between the approaching surfaces at a ∼2 μm distance.[14] Here in Figure 4c, the frictional force between a sliding SH probe on an SH substrate is ∼20% smaller in water than in air. This modest decrease in frictional force in water suggests that any gain in adhesive forces for such superhydrophobic systems is outweighed by other factors related to the simultaneous advancing (of the trailing edge) and receding (of the leading edge) of the water from the superhydrophobic interfaces during sliding.

In contrast to the hydrocarbon film-coated probes, water has a significant effect for the polymer films being tested with the control probe, which is hydrophilic. In water, the friction of the PM substrate is decreased from 17.4 ± 2.7 to 12.7 ± 2.9 mN, while the SH substrate frictional forces decreased from 18.7 ± 3.9 to 10.5 ± 1.6 mN (Figure 4d). Adsorbed water can form a lubricating film on the hydrophilic control probe and separate sliding surfaces[41] during the underwater testing. This water layer would lower the shear and decrease the adhesion between the probe and substrate,[42] reducing friction forces. Fluid lubrication due to water has been seen before for microtribometry, as friction was decreased for a polymer brush system when testing was done in water rather than in dry N_2.[42] The control/C18 substrate system was unaffected by the water

dx.doi.org/10.1021/jp305527h | J. Phys. Chem. C 2012, 116, 21795−21801

layer, since the C18 monolayer already provides a smooth low-friction surface.

CONCLUSIONS

Microtribometry tests were performed on various polymer-coated substrates to examine polymer/polymer friction and investigate the tribological effect of plowing and topography. As opposed to hydrocarbon monolayers, the frictional performance of the PM and SH substrate films was dependent on the surface energy of the probe, as the lubricating properties of the C18 probe monolayer[18,23,34,35] diminished the plowing force and shear strength. When polymer probes were used on the polymer substrates, the ratcheting mechanism was the dominant influence, as the highest friction forces occurred when microscale asperities were present. In addition, tribometry tests were performed with the substrates submerged under water to examine the influence of hydrophobic interactions on microscale friction, the effectiveness of an entrapped air lubrication layer at an SH/SH interface, and the frictional benefit of a chemisorbed water layer. For the C18, PM, and SH probes, the water environment had little influence on the frictional results, suggesting that, at the loads and speeds tested, hydrophobic interactions as well as an entrapped air layer between the SH substrate/SH probe do not significantly influence the lubrication properties. The unmodified probe, in contrast, showed decreased frictional forces for the polymer substrates in the water environment. This decrease was attributed to a chemisorbed water layer on the hydrophilic probe, which lowered the shear and decreased the adhesion between the probe and substrate.

AUTHOR INFORMATION

Corresponding Author

*E-mail: kane.g.jennings@vanderbilt.edu. Phone: (615) 322-2707. Fax: (615) 343-7951.

Notes

The authors declare no competing financial interest.

ACKNOWLEDGMENTS

This work was supported by the Office of Naval Research via Grants N00014-06-1-0624, N00014-09-1-0334, and N00014-07-1-0843 and the State of Tennessee.

REFERENCES

(1) Jia, B. -B.; Li, T. -S.; Liu, X. -J.; Cong, P. -H. *Wear* **2007**, *262*, 1353−1359.
(2) Mate, C. M. *Tribology on the Small Scale: A Bottom Up Approach to Friction, Lubrication, and Wear*; Oxford University Press: New York, 2008; p 333.
(3) Lavielle, L. *Wear* **1991**, *151*, 63−75.
(4) *Modern Tribology Handbook*; Bhusan, B., Ed.; CRC Press: Boca Raton, FL, 2001.
(5) Hoffmann, H.; Mayer, U.; Krischanitz, A. *Langmuir* **1995**, *11*, 1304−1312.
(6) Guo, W.; Jennings, G. K. *Langmuir* **2002**, *18*, 3123−3126.
(7) Tuberquia, J. C.; Nizamidin, N.; Jennings, G. K. *Langmuir* **2010**, *26*, 14039−14046.
(8) Tuberquia, J. C.; Nizamidin, N.; Harl, R. R.; Albert, J.; Hunter, J.; Rogers, B. R.; Jennings, G. K. *J. Am. Chem. Soc.* **2010**, *132*, 5725−5734.
(9) Sweeting, O. J. *The Science and Technology of Polymer Films*; John Wiley & Sons: New York, 1968.
(10) Heuberger, M.; Luengo, G.; Israelachvili, J. N. *J. Phys. Chem. B* **1999**, *103*, 10127−10135.
(11) Stehling, F. C.; Mandelkern, L. *Macromolecules* **1970**, *3*, 242−252.
(12) Clear, S. C.; Nealey, P. F. *J. Colloid Interface Sci.* **1999**, *213*, 238−250.
(13) Noy, A.; Frisbie, C. D.; Rozsnyai, L. F.; Wrighton, M. S.; Lieber, C. M. *J. Am. Chem. Soc.* **1995**, *117*, 7943−7951.
(14) Singh, S.; Houston, J.; van Swol, F.; Brinker, C. J. *Nature* **2006**, *442*, 526−526.
(15) Rothstein, J. P. *Annu. Rev. Fluid Mech.* **2010**, *42*, 89−109.
(16) Meyer, E. E.; Rosenberg, K. J.; Israelachvili, J. *Proc. Natl. Acad. Sci. U.S.A.* **2006**, *103*, 15739−15746.
(17) Bäurle, L.; Szabó, D.; Fauve, M.; Rhyner, H.; Spencer, N. D. *Tribol. Lett.* **2006**, *24*, 77−84.
(18) Vilt, S. G.; Leng, Z.; Booth, B. D.; McCabe, C.; Jennings, G. K. *J. Phys. Chem. C* **2009**, *113*, 14972−14977.
(19) Black, T. H. *Aldrichimica Acta* **1983**, *16*, 3−10.
(20) Tompkins, H. G.; McGahan, W. A. *Spectroscopic Ellipsometry and Reflectometry: A User's Guide*; John Wiley & Sons: New York, 1999.
(21) Mark, J. E. *Polymer Data Handbook*, 2nd ed.; Oxford University Press: New York, 2009.
(22) Booth, B. D.; Vilt, S. G.; Ben Lewis, J.; Rivera, J. L.; Buehler, E. A.; McCabe, C.; Jennings, G. K. *Langmuir* **2011**, *27*, 5909−5917.
(23) Booth, B. D.; Vilt, S. G.; McCabe, C.; Jennings, G. K. *Langmuir* **2009**, *25*, 9995−10001.
(24) Tillman, N.; Ulman, A.; Schildkraut, J. S.; Penner, T. L. *J. Am. Chem. Soc.* **1988**, *110*, 6136−6144.
(25) Depalma, V.; Tillman, N. *Langmuir* **1989**, *5*, 868−872.
(26) Tuberquia, J. C.; Song, W. S.; Jennings, G. K. *Anal. Chem.* **2011**, *83*, 6184−6190.
(27) Bowden, F. P.; Tabor, D. *Br. J. Appl. Phys.* **1966**, *17*, 1521.
(28) Nosonovsky, M.; Bhushan, B. *Mater. Sci. Eng., R* **2007**, *58*, 162−193.
(29) Pietrement, O.; Troyon, M. *Langmuir* **2001**, *17*, 6540−6546.
(30) Masuko, M.; Miyamoto, H.; Suzuki, A. *Tribol. Int.* **2007**, *40*, 1587−1596.
(31) Sambasivan, S.; Hsieh, S.; Fischer, D. A.; Hsu, S. M. *J. Vac. Sci. Technol., A* **2006**, *24*, 1484−1488.
(32) Gaur, U.; Wunderlich, B. *Macromolecules* **1980**, *13*, 445−446.
(33) Maeda, N.; Chen, N.; Tirrell, M.; Israelachvili, J. N. *Science* **2002**, *297*, 379−382.
(34) Ren, S.; Yang, S.; Zhao, Y.; Zhou, J.; Xu, T.; Liu, W. *Tribol. Lett.* **2002**, *13*, 233−239.
(35) Baker, M. A.; Li, J. *Surf. Interface Anal.* **2006**, *38*, 863−867.
(36) Song, Y.; Nair, R. P.; Zou, M.; Wang, Y. A. *Thin Solid Films* **2010**, *518*, 3801−3807.
(37) Karuppiah, K. S. K.; Bruck, A. L.; Sundararajan, S.; Wang, J.; Lin, Z. Q.; Xu, Z. H.; Li, X. D. *Acta Biomater.* **2008**, *4*, 1401−1410.
(38) Myshkin, N. K.; Petrokovets, M. I.; Kovalev, A. V. *Tribol. Int.* **2005**, *38*, 910−921.
(39) Choi, C. H.; Kim, C. J. *Phys. Rev. Lett.* **2006**, *96*, 066001.
(40) Cottin-Bizonne, C.; Barrat, J. L.; Bocquet, L.; Charlaix, E. *Nat. Mater.* **2003**, *2*, 237−240.
(41) Ku, I. S. Y.; Reddyhoff, T.; Holmes, A. S.; Spikes, H. A. *Wear* **2011**, *271*, 1050−1058.
(42) Ishikawa, T.; Kobayashi, M.; Takahara, A. *ACS Appl. Mater. Interfaces* **2010**, *2*, 1120−1128.